

Supporting Information

Covalent Organic Framework based Microspheres as Anode Material for Rechargeable Sodium Batteries

Bidhan Chandra Patra, ^a Sabuj Kanti Das, ^{b, ‡} Arnab Ghosh, ^{c, ‡} Anish Raj K, ^{c, ‡} Parikshit Moitra, ^d Matthew Addicoat, ^e Sagar Mitra, ^{, c} Asim Bhaumik, ^{*, b} Santanu Bhattacharya ^{*, a} and Anirban Pradhan ^{*, a}*

^aDirector's Research Unit, Indian Association for the Cultivation of Science, Jadavpur, Kolkata 700032, INDIA. E-mail: msap5@iacs.res.in (A.P.), director@iacs.res.in (S.B.)

^bDepartment of Materials Science, Indian Association for the Cultivation of Science, Jadavpur, Kolkata 700032, INDIA. E-mail: msab@iacs.res.in (A.B.)

^cDepartment of Energy Science and engineering, Indian Institute of Technology, Bombay, Powai, Mumbai, Maharashtra 400076, INDIA. E-mail: sagar.mitra@iitb.ac.in (S.M.)

^dTechnical Research Centre, Indian Association for the Cultivation of Science, Jadavpur, Kolkata 700032, INDIA.

^eSchool of Science and Technology, Nottingham Trent University, Clifton Lane, Nottingham, NG11 8NS, UK.

Section	Content
Section S1	General information
Section S2	Synthesis and characterization of TFPB-TAPT COF
Section S3	Computational details of powder X-ray diffraction for TFPB-TAPT COF
Section S4	SEM image and TGA plot of TFPB-TAPT COF
Section S5	Calculation of theoretical specific capacity for TFPB-TAPT COF
Section S6	Ex-situ HRTEM analyses of electrode materials after cycling
Section S7	Calculation of sodium-ion diffusion coefficient
Section S7	Performance of TFPB-TAPT COF anode in lithium batteries

Section S1: General information

FT-IR spectra of the synthesized samples were recorded using a Nicolet MAGNA-FT IR 750 Spectrometer Series II. Solid state ^{13}C CP MAS NMR spectrum of **TFPB-TAPT** was recorded in a 500 MHz BrukerAvance III spectrometer at a MAS frequency of 10 kHz. X-Ray diffraction patterns of the powder samples were obtained with a Bruker AXS D-8 Advanced SWAX diffractometer using $\text{Cu-K}\alpha$ (0.15406 nm) radiation. The N_2 adsorption/desorption isotherms of the sample was recorded using an Autosorb 1C (Quantachrome, USA) at 77 K. The sample was first degassed at 120 °C for overnight and set for measurement. Pore size distribution (PSD) was calculated by using NLDFT considering the carbon/slit-cylindrical pore model. Scanning electron microscopic analysis was performed with a JEOL JEM 6700F field-emission scanning electron microscope (FESEM). High resolution Transmission electron microscopy (HR-TEM) images of the synthesized polymer were obtained using a JEOL JEM 2010 transmission electron microscope operated at 200 kV. The sample was dispersed in isopropanol and drop casted on the copper grid TEM window. X-ray photoelectron spectroscopy (XPS) was performed on an Omicron nanotech operated at 15 kV and 20 mA. Thermal analyzer TA-SDT Q-600 was used for thermogravimetric (TG) by heating the samples from room temperature to 800 °C with a heating rate of 10 °C min^{-1} under N_2 atmosphere.

Section S2: Synthesis and characterization of TFPB-TAPT COF

Synthesis of 1, 3, 5-tris (4-formyl phenyl) benzene (TFPB)

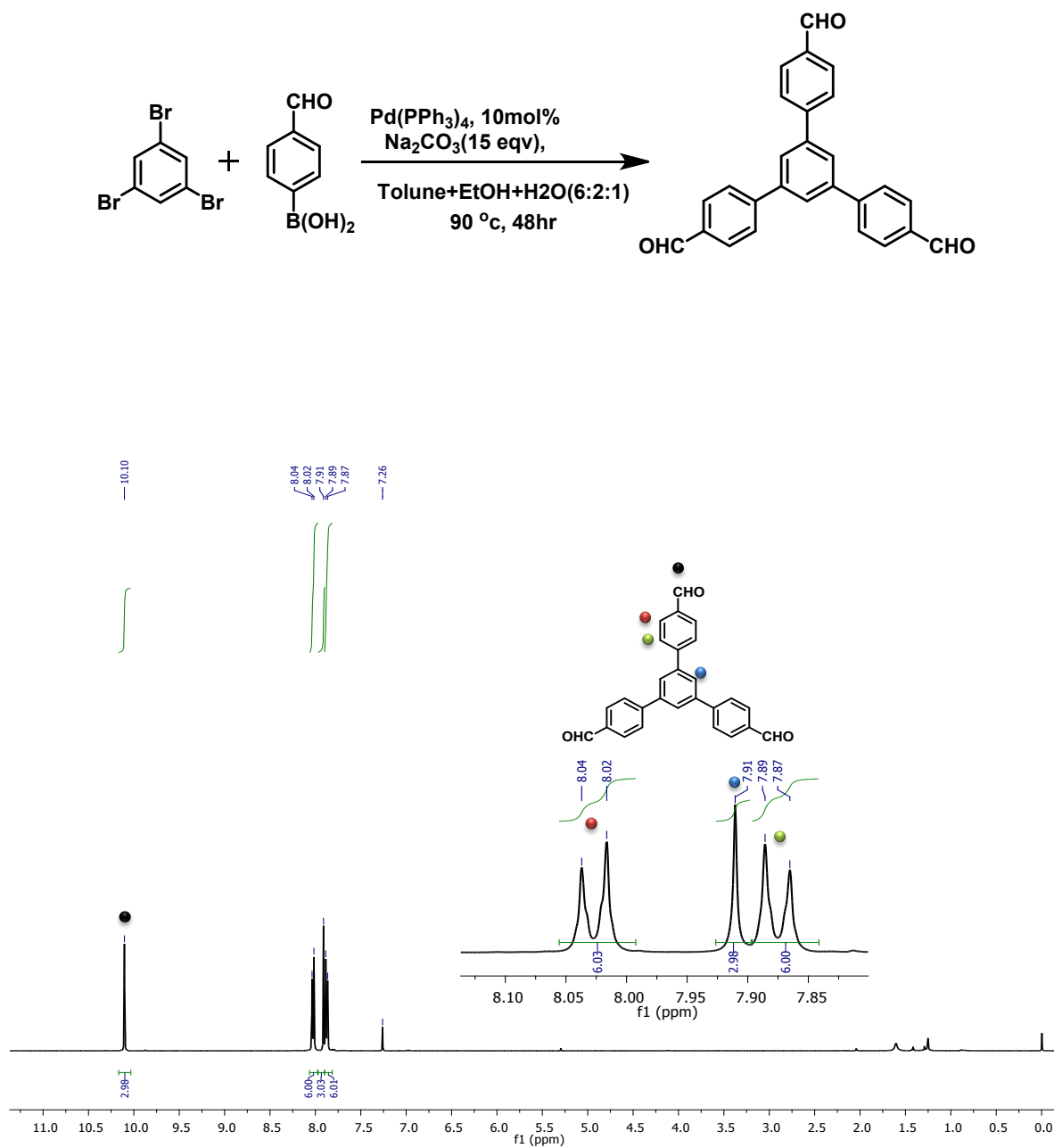


Figure S1. ¹H NMR of 1, 3, 5-tris (4 formyl phenyl) benzene (TFPB).

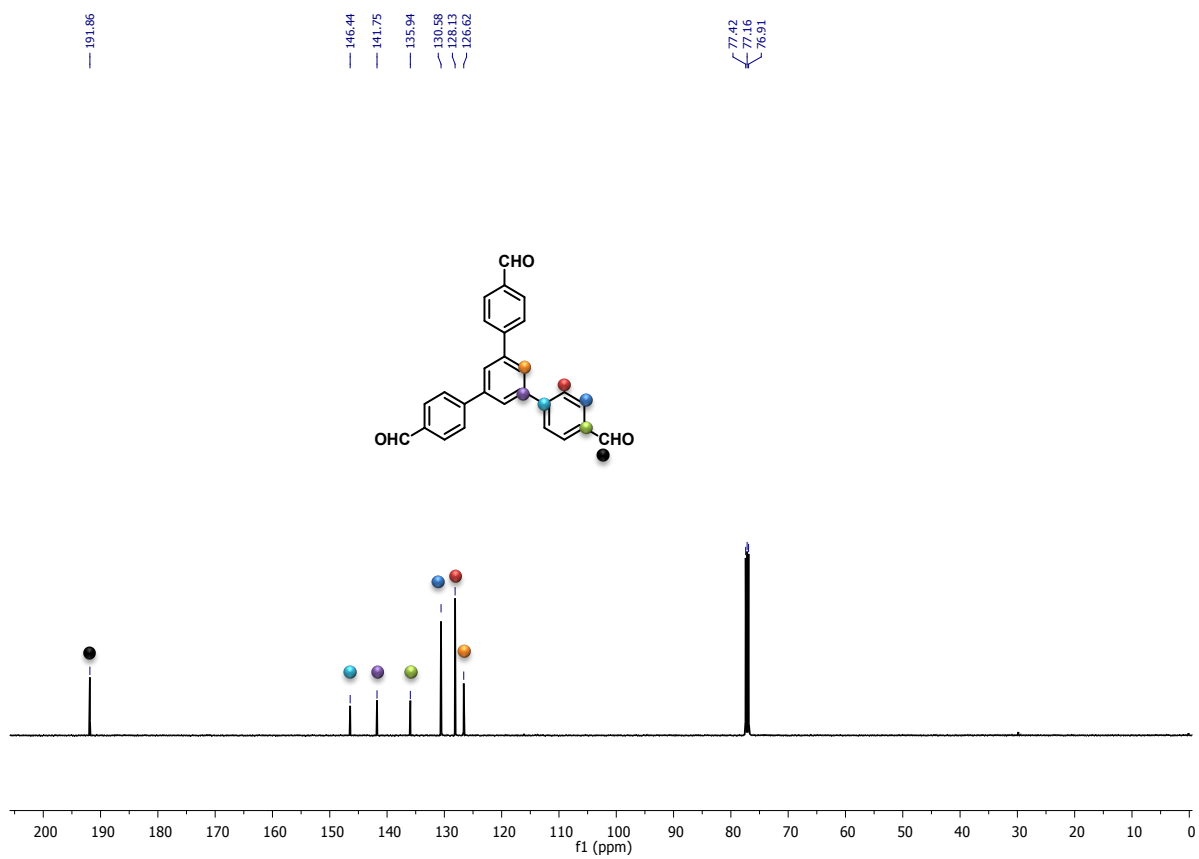


Figure S2. ^{13}C NMR of 1, 3, 5-tris (4 formyl phenyl) benzene (TFPB).

Synthesis of 2, 4, 6-tris (4-aminophenyl)-1, 3, 5-triazine (TAPT)

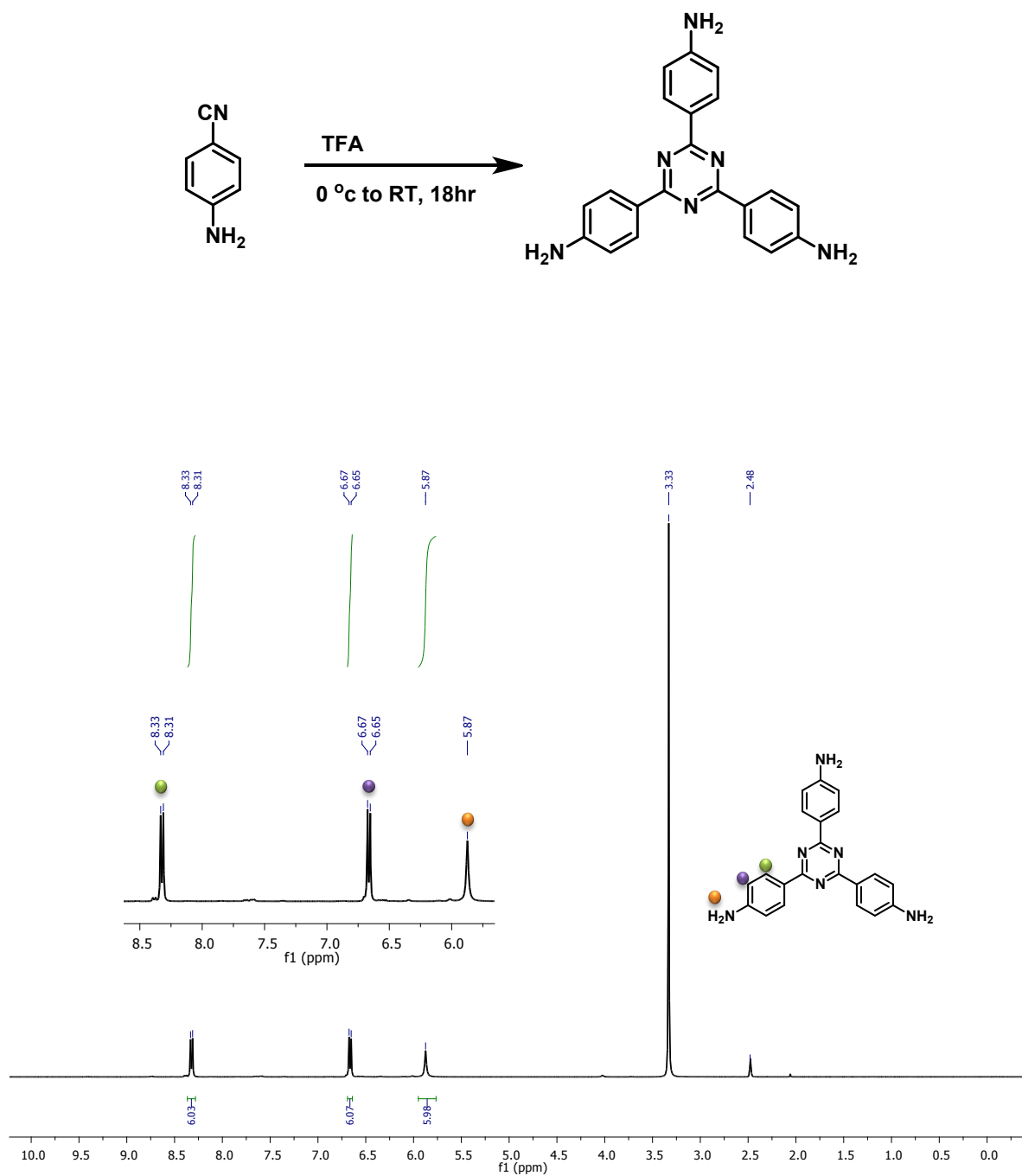


Figure S3. ¹H NMR of 2, 4, 6-tris (4-aminophenyl)-1, 3, 5-triazine (TAPT).

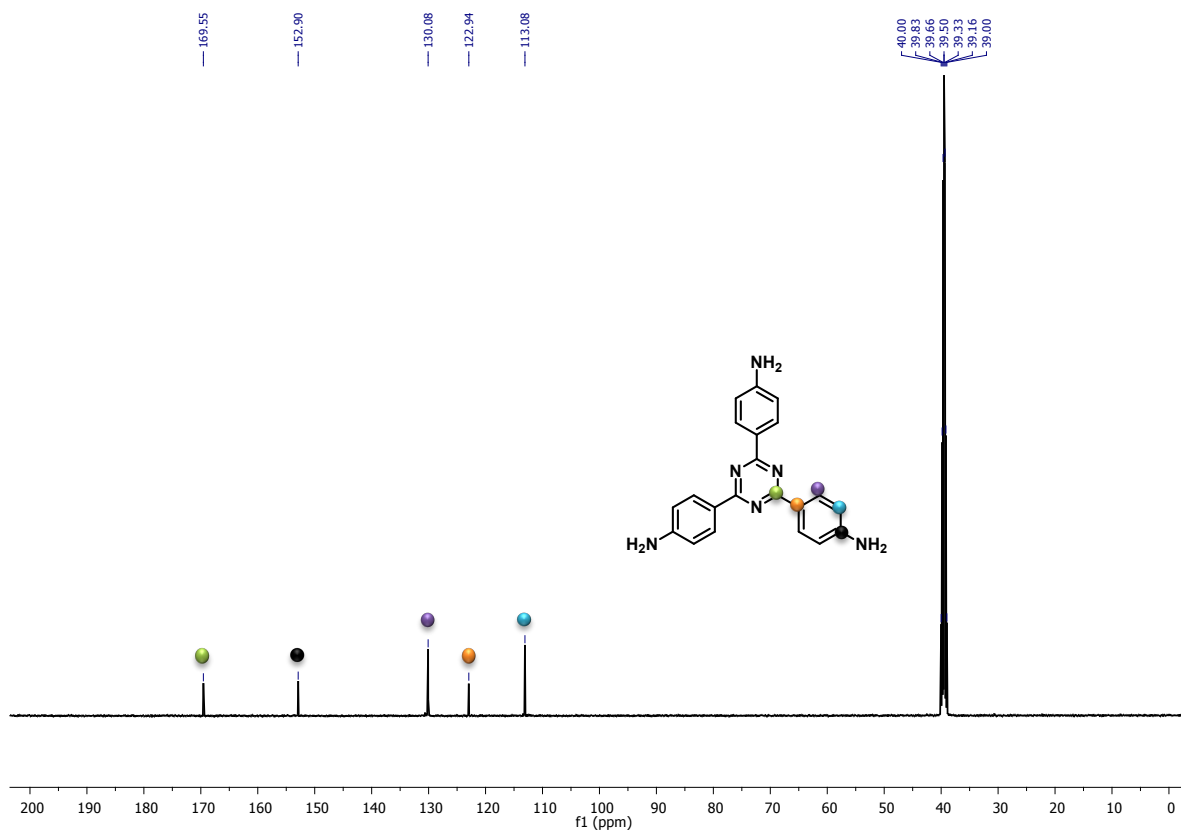


Figure S4. ^{13}C NMR of 2,4,6-tris(4-aminophenyl)-1,3,5-triazine (TAPT).

Section S3: Computational details of powder X-ray diffraction for TFPB-TAPT COF

Table S1. For the normal stacking structures

	Interlayer distance (Å)	Total Energy (kcal/mole)	LJ energy (a.u.)	Per layer stabilization (kcal/mole)	HOMO-LUMO gap (eV)
Monolayer		-107.674677	0.4732		2.518
AA	3.49	-215.548056	0.7351	-62.34	2.179
SlipAA-x	3.56	-215.578028	0.7238	-71.75	2.474
SlipAA-xy	3.60	-215.576896	0.7217	-71.39	2.359
AB	3.12	-215.4608188	0.8367	-34.97	2.266

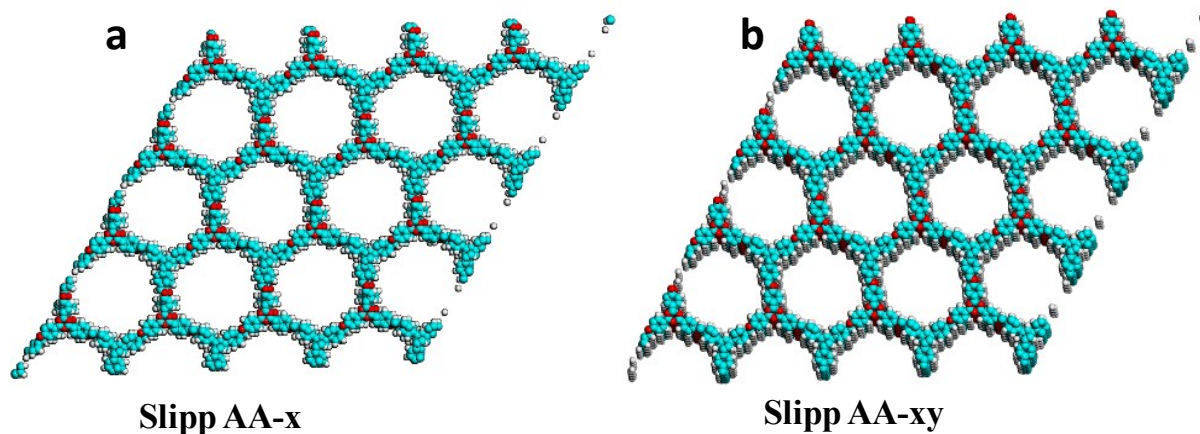


Figure S5. Structure of Slipped AA-x and Slipped AA-xy of TFPB-TAPT COF.

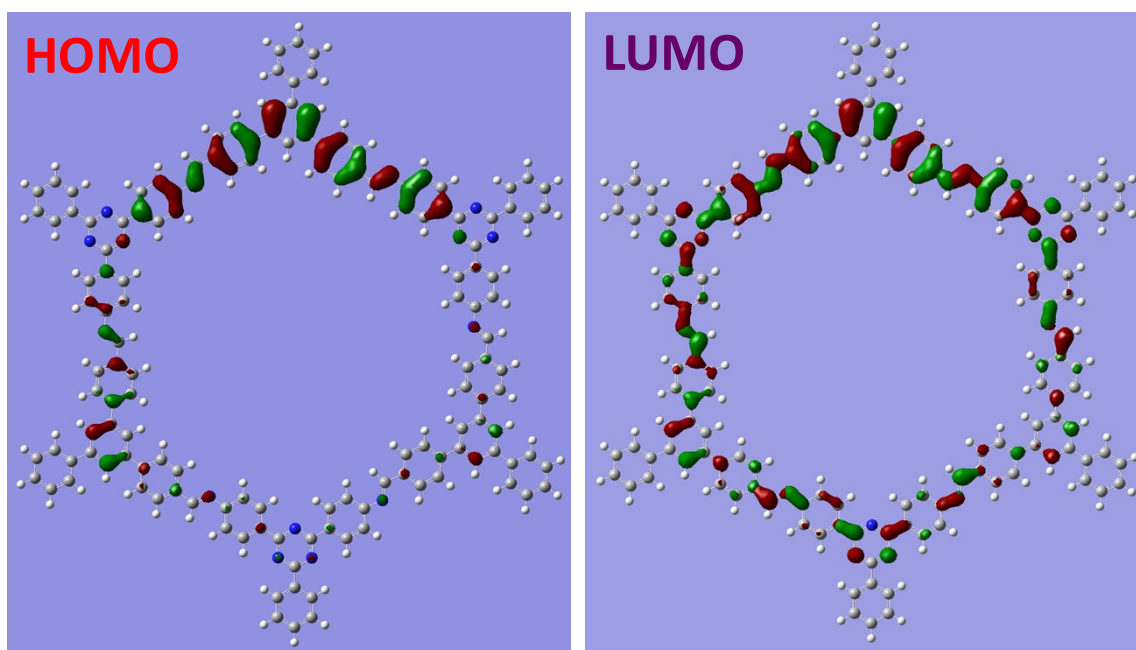


Figure S6. HOMO-LUMO diagram of TFPB-TAPT COF.

Table S2. For the reverse stacked structures

	Interlayer distance (Å)	Total Energy (kcal/mole)	LJ energy (a.u.)	Per layer stabilization (kcal/mole)	HOMO-LUMO gap (eV)
Monolayer		-107.674677	0.4732		2.518
AA	3.48	-215.554517	0.7351	-64.37	2.236
SlipAA-x	3.37	-215.561999	0.7344	-66.72	2.345
SlipAA-xy	3.54	-215.573835	0.7294	-70.43	2.414
AB	3.06	-215.4563012	0.8404	-33.56	2.459

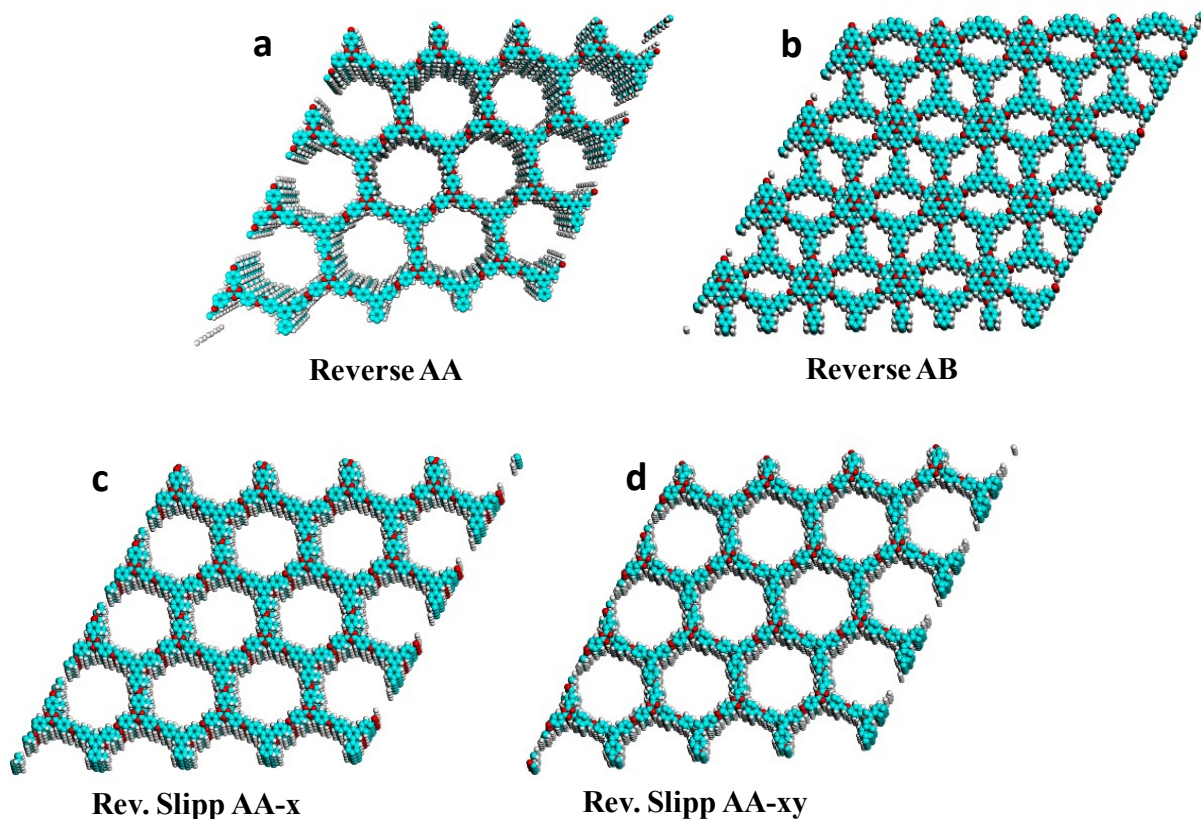


Figure S7. Crystal structure of **TFPB-TAPT** COF at different reverse mode.

Table S3. Fractional atomic coordinates for the unit cell of **TFPB-TAPT**

TFPB-TAPT; Triclinic; <i>P1</i>			
$a = 25.789001\text{\AA}; b = 25.7835\text{\AA}; c = 7.20107\text{\AA}$			
$\alpha = 77.628182, \beta = 90.907426, \gamma = 61.193553$			
Atom list	x	y	z
C1	0.86923	0.27157	0.98416
C2	0.90491	0.29922	0.98412
C3	0.88144	0.35896	0.00686
C4	0.82044	0.39232	0.0241
C5	0.78296	0.36702	0.01707
C6	0.80813	0.3064	7.4E-4
H1	0.95192	0.27446	0.96128
H2	0.80219	0.43816	0.04955
H3	0.77903	0.28627	0.99889
C7	0.71788	0.40487	0.02024

C8	0.68301	0.37952	0.10119
C9	0.68857	0.46833	0.93376
C10	0.62143	0.41586	0.09338
H4	0.70428	0.33049	0.17399
C11	0.62709	0.50469	0.92617
H5	0.71379	0.48977	0.86562
C12	0.59224	0.47911	0.00434
H6	0.59519	0.39504	0.15694
H7	0.60552	0.5539	0.85546
C13	0.92027	0.38639	0.01323
C14	0.89778	0.4496	0.93524
C15	0.98055	0.35022	0.09875
C16	0.93382	0.47568	0.94415
H8	0.85144	0.47899	0.86288
C17	0.01649	0.37637	0.10968
H9	0.99974	0.30081	0.16184
C18	0.99373	0.43958	0.03297
H10	0.91555	0.52498	0.882
H11	0.06312	0.34718	0.17972
C19	0.89571	0.20733	0.9703
C20	0.85975	0.18287	0.9261
C21	0.95829	0.16753	0.00653
C22	0.88489	0.12161	0.9236
H12	0.81089	0.21194	0.89129
C23	0.98361	0.1066	8.1E-4
H13	0.98846	0.18378	0.04411
C24	0.94733	0.08218	0.96114
H14	0.85545	0.10406	0.88938
H15	0.03244	0.07666	0.03071
C25	0.97347	0.01772	0.95931
H16	0.94072	0.00134	0.94303
C26	0.03141	0.46712	0.04731
H17	0.07667	0.4365	0.13624
N1	0.01236	0.52386	0.96501
N2	0.03067	0.98305	0.97558
C27	0.05827	0.92102	0.97579
C28	0.02735	0.88987	0.94681
C29	0.12148	0.88798	0.00816
C30	0.05902	0.82788	0.95302
H18	0.97824	0.91383	0.91843
C31	0.15288	0.82595	0.01315
H19	0.14581	0.91182	0.03131

C32	0.12203	0.79491	0.98609
H20	0.03487	0.80375	0.9306
H21	0.20207	0.80073	0.03964
C33	0.15365	0.72934	0.98914
C34	0.24001	0.6394	7.8E-4
C35	0.14916	0.64309	0.97767
N3	0.12013	0.70277	0.97697
N4	0.21376	0.69893	0.00263
N5	0.20903	0.61024	0.98793
C36	0.114	0.61214	0.97028
C37	0.14183	0.55111	0.95552
C38	0.05217	0.64273	0.98134
C39	0.10932	0.5209	0.95524
H22	0.18986	0.52736	0.94329
C40	0.01914	0.61313	0.97954
H23	0.03022	0.69041	0.99286
C41	0.04757	0.5514	0.97042
H24	0.13166	0.47375	0.93887
H25	0.97117	0.63693	0.99202
C42	0.30566	0.60386	0.01412
C43	0.33369	0.54222	0.00525
C44	0.3415	0.63006	0.0383
C45	0.39562	0.50767	0.02026
H26	0.30586	0.5216	0.98589
C46	0.4035	0.59601	0.05185
H27	0.32007	0.67789	0.04806
C47	0.43137	0.53437	0.041
H28	0.41691	0.45991	0.01033
H29	0.43057	0.61704	0.0758
N6	0.49355	0.49722	0.05827
C48	0.52728	0.51819	0.98712
H30	0.50874	0.56707	0.90297
C49	0.88253	0.2782	0.49016
C50	0.91825	0.30564	0.4953
C51	0.89413	0.36625	0.51061
C52	0.83252	0.40036	0.51866
C53	0.79519	3/8	0.50821
C54	0.82082	0.31397	0.49637
H31	0.96608	0.27983	0.48327
H32	0.81363	0.44685	0.53929
H33	0.79147	0.29436	0.48929
C55	0.72976	0.41309	0.50396

C56	0.69452	0.38776	0.58125
C57	0.70064	0.47646	0.41619
C58	0.63292	0.42418	0.57167
H34	0.71549	0.3387	0.65316
C59	0.63903	0.5129	0.40567
H35	0.72617	0.49782	0.34999
C60	0.60404	0.48743	0.48305
H36	0.60639	0.40352	0.63352
H37	0.61762	0.56207	0.33463
C61	0.93281	0.39383	0.51813
C62	0.91073	0.45676	0.43571
C63	0.99264	0.35813	0.60824
C64	0.94668	0.48298	0.44418
H38	0.86474	0.48589	0.36035
C65	0.02865	0.38431	0.617
H39	0.01132	0.30912	0.67722
C66	0.00631	0.44723	0.53557
H40	0.92861	0.53208	0.37886
H41	0.07499	0.35539	0.68991
C67	0.90927	0.2136	0.47957
C68	0.87344	0.18871	0.43809
C69	0.9719	0.17395	0.51434
C70	0.89868	0.12754	0.43455
H42	0.8245	0.21736	0.40599
C71	0.99731	0.11301	0.50864
H43	0.00213	0.19035	0.55012
C72	0.96116	0.08839	0.46959
H44	0.86925	0.10985	0.40161
H45	0.04619	0.08329	0.53724
C73	0.98734	0.02407	0.46595
H46	0.95462	0.00767	0.44969
C74	0.04407	0.47479	0.54855
H47	0.08897	0.4445	0.63996
N7	0.02553	0.53117	0.4629
N8	0.04453	0.98952	0.48105
C75	0.07205	0.92749	0.48114
C76	0.0411	0.89633	0.45284
C77	0.13527	0.89443	0.51315
C78	0.07271	0.83436	0.45887
H48	0.99199	0.9203	0.4249
C79	1/6	0.83238	0.51835
H49	0.15965	0.91827	0.53589

C80	0.13572	0.80138	0.49148
H50	0.04853	0.81025	0.43668
H51	0.21583	0.80717	0.54452
C81	0.16729	0.73588	0.49358
C82	0.25352	0.646	0.50386
C83	0.16266	0.64982	0.4804
N9	0.13373	0.70939	0.48115
N10	0.22738	0.7055	0.50606
N11	0.22251	0.61693	0.49046
C84	0.1274	0.61908	0.47112
C85	0.15518	0.55813	0.4557
C86	0.06549	0.64987	0.48072
C87	0.12255	0.52809	0.45385
H52	0.20326	0.53433	0.44411
C88	0.03237	0.6204	0.47777
H53	0.04357	0.69755	0.49226
C89	0.06078	0.55868	0.46846
H54	0.14482	0.481	0.43702
H55	0.98436	0.6443	0.48944
C90	0.31916	0.61042	0.51713
C91	0.34717	0.54862	0.50995
C92	0.35489	0.63688	0.53884
C93	0.40903	0.51427	0.52255
H56	0.31936	0.52776	0.49368
C94	0.4168	0.60317	0.54865
H57	0.33346	0.68474	0.54831
C95	0.44453	0.54157	0.53762
H58	0.43038	0.46643	0.51356
H59	0.4439	0.6245	0.56855
N12	0.50659	0.50518	0.54924
C96	0.53907	0.5262	0.46738
H60	0.51943	0.57452	0.37662

Section S4: SEM image and TGA plot of TFPB-TAPT COF

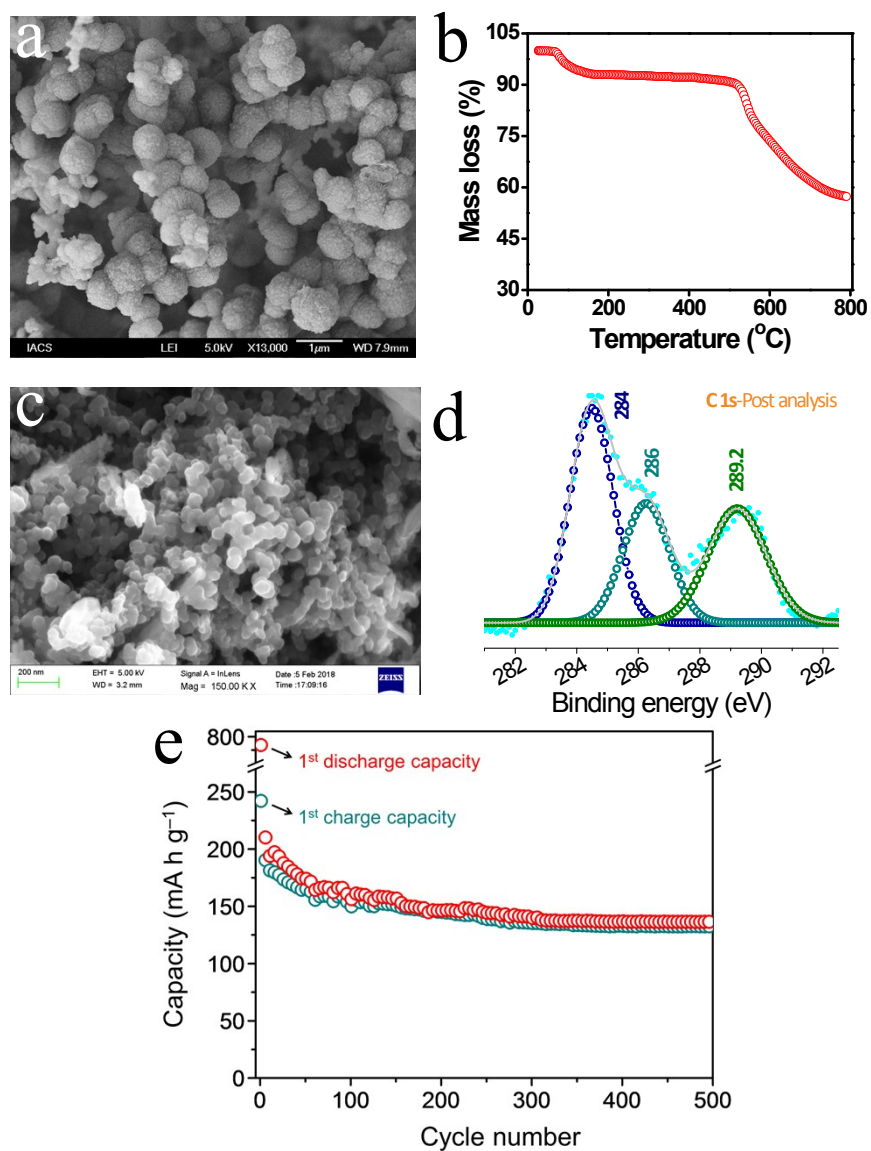


Figure S8. (a, c) SEM image of the TFPB-TAPT COF before and after cycling, respectively. (b) TGA plot of the TFPB-TAPT COF (d) C1s XPS spectrum of TFPB-TAPT COF after cycling. (e) Long-term cycling performance of TFPB-TAPT COF in sodium batteries.

Section S5: Calculation of theoretical specific capacity for TFPB-TAPT COF

Theoretical specific capacity of the **TFPB-TAPT** electrode was calculated by the following formula:^{1,2}

$$C_t = \frac{F \times 1000}{M \times 3600} \text{ mA h g}^{-1} \text{ unit.}$$

Where, C_t = theoretical capacity, F = Faraday constant and M = molecular weight per active site.

$$M = \frac{\text{Molecular weight per mole}}{\text{No of active site for sodium ion adsorption}}$$

Molecular weight of per unit **TFPB-TAPT** COF is 1380 g mol^{-1} .

$$\text{Thus, } M = \frac{1380}{12} = 115 \text{ g (considering 1 Na}^+ \text{ /-C=N bond)}$$

Hence, the theoretical specific capacity (C_t) is $233.05 \text{ mA h g}^{-1}$.

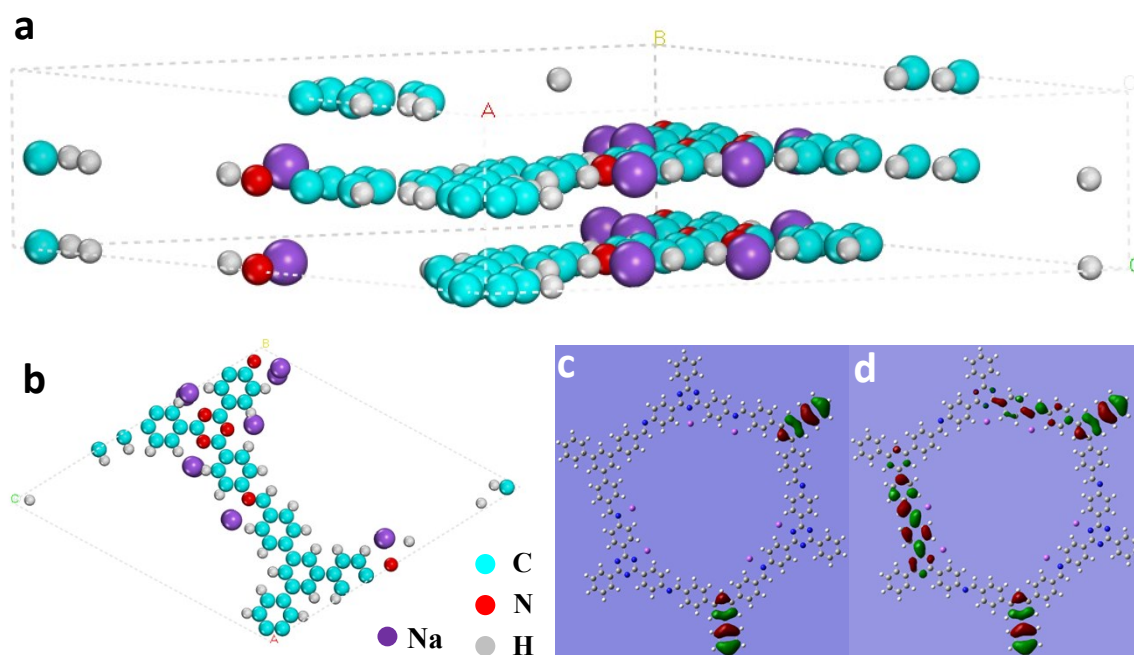


Figure S9. Side view (a) and top view (b) of one unit cell of the sodium ion inserted **TFPB-TAPT** COF Crystal, HOMO (c) and LUMO (d) of the **TFPB-TAPT** COF after sodium ion insertion.

Section S6: Ex-situ TEM analyses of electrode materials after cycling

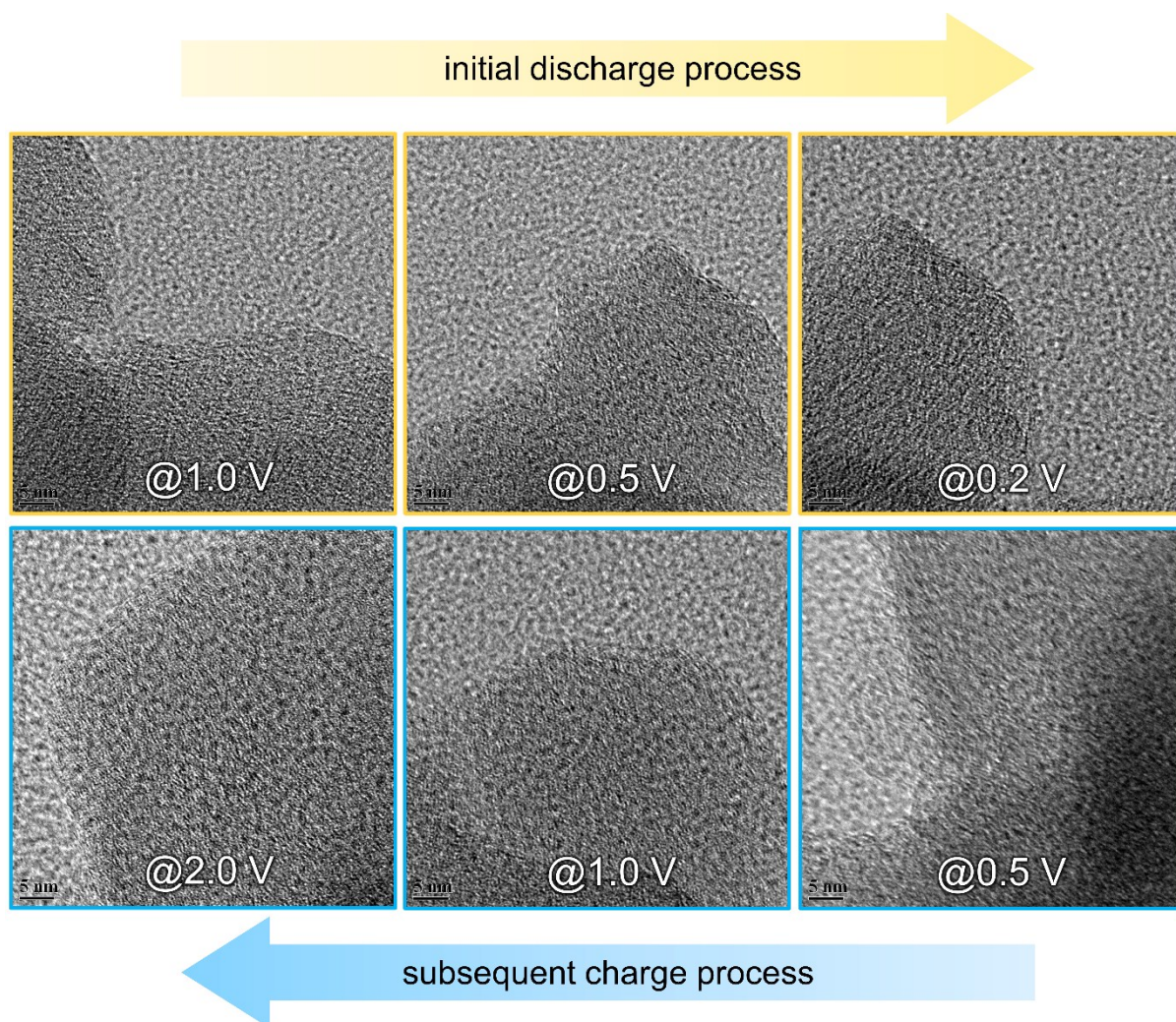


Figure S10. HRTEM images of electrode materials stopping the cells at different voltages during initial discharge and subsequent charge processes.

Section S7: Calculation of sodium-ion diffusion coefficient

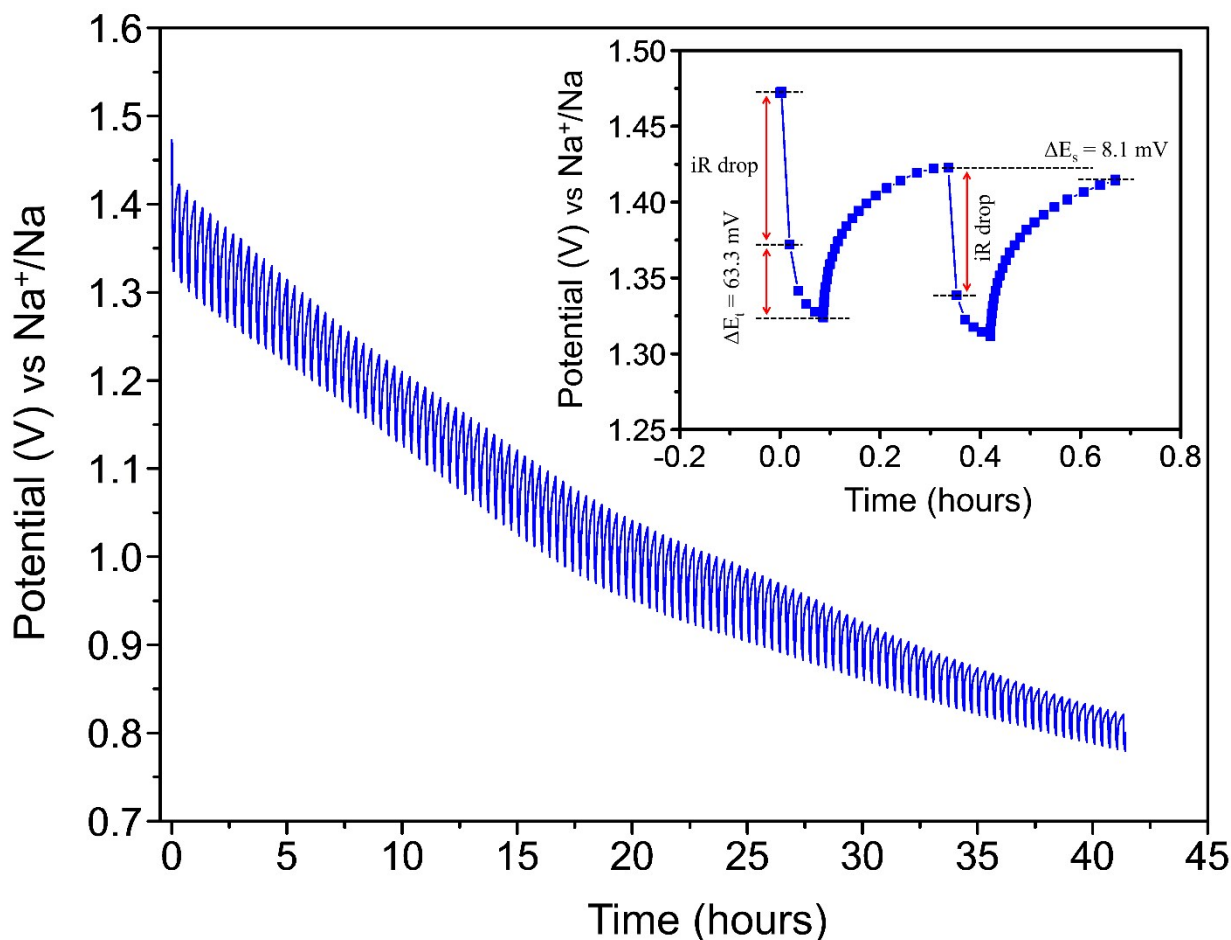


Figure S11. GITT profiles of the **TFPB-TAPT** COF anode in sodium batteries. Each discharge step is composed of 5 minutes of galvanostatic discharge at the current rate of 50 mA g⁻¹, followed by 15 minutes of relaxation time.

From the GITT experiment ion-diffusion coefficient can be calculated using the following equation:

$$D = \frac{4}{\pi\tau} \left(\frac{n_M V_M}{S} \right)^2 \left(\frac{\Delta E_s}{\Delta E_t} \right)^2 \dots\dots\dots \text{Eq. 1}$$

Where, τ is the duration of the current pulse (in seconds); n_M and V_M are the molar mass (mol) and volume (cm³/mol) of the active material; S is area of the electrode (cm²); ΔE_s is the steady-state voltage change due to the current pulse and ΔE_t is the voltage change during the

constant current pulse, eliminating the iR drop. The **TFPB-TAPT** COF anode is consisted of spherical particles of radius R_s . So, the Eq. 1 may be written as

$$D = \frac{4}{\pi\tau} \left(\frac{R_s}{3}\right)^2 \left(\frac{\Delta E_s}{\Delta E_t}\right)^2 \dots\dots\dots \text{Eq. 2}$$

The GITT profile of the **TFPB-TAPT** COF anode during discharge is shown in Figure S11. Each discharge step is composed of 5 minutes of galvanostatic discharge, followed by 15 minutes of relaxation time. The first two discharge steps are chosen to estimate the value of ion-diffusion coefficient (Figure S11, inset). The values of ΔE_s and ΔE_t were estimated to be 8.1 mV and 63.3 mV. Now, we can calculate the diffusion coefficient putting the values of each parameter in Eq. 2.

$$\tau \text{ (duration of the current pulse)} = 300 \text{ sec,}$$

$$R_s \text{ (radius of COF microsphere)} = 285 \text{ nm or } 2.85 \times 10^{-5} \text{ cm,}$$

$$\Delta E_s \text{ (steady-state voltage change due to the current pulse)} = 8.1 \text{ mV,}$$

$$\Delta E_t \text{ (voltage change during the constant current pulse)} = 63.3 \text{ mV.}$$

$$\text{Hence, } D = 6.275 \times 10^{-15} \text{ cm}^2 \text{ s}^{-1}.$$

Section S8: Performance of TFPB-TAPT COF anode in lithium batteries

Cell assembly and electrochemical characterization

To investigate the electrochemical performances of **TFPB-TAPT** COF with respect to lithium, CR2016 coin cells were assembled using lithium metal as counter/reference electrode. Celgard 2400 soaked with 40 μL of electrolyte comprised of 1 M LiPF_6 in 1:1 (v/v) mixture of ethylene carbonate (EC) and dimethyl carbonate (DMC) was used as separator. Cyclic voltammetry (CV) study was carried out at a scan rate of 0.02 mV s^{-1} within the potential window 0.001-3.0 V (vs Li^+/Li). The charge-discharge experiments were carried out within the potential range 0.05-2.6 V (vs Li^+/Li) at different current rates. The capacities were evaluated based on the mass of active material present in the electrode (*i.e.*, 1.65 mg cm^{-2}). All the electrochemical measurements were carried out at the constant temperature of $20 \text{ }^\circ\text{C}$.

Results and discussion

TFPB-TAPT COF exhibited a very good reversible redox behaviour with respect to lithium, as revealed by cyclic voltammetry experiment. Figure S12a represents the first scan of cyclic voltammetry study of **TFPB-TAPT** in the voltage range of 0.001-3.0 V versus Li⁺/Li redox system at 0.02 mV s⁻¹ scan rate. During first cathodic scan, a sharp peak at 1.7 V and a broad peak located at the potential zone of 0.5-1.5 V were obtained. These two peaks are associated with successive two steps of Li⁺ ion insertion into **TFPB-TAPT** COF. However, the broad peak at the lower potential is also accompanied by insertion of Li⁺ ion into conductive super P carbon additive as well as decomposition of electrolyte to form stable solid electrolyte interphase (SEI). On the reverse scan, three peaks were observed, an intense broad peak at 1.05 V, a weak peak at 1.95 V and an intense sharp peak at 2.35 V; all are related to Li⁺ ion de-intercalation processes. However, during second cycle onwards, the nearly identical nature of CV curves (Figure S12b) implies excellent Li⁺ ion storage reversibility of **TFPB-TAPT** COF. Charge-discharge cycling performance of **TFPB-TAPT** COF at the current rate of 30 mA g⁻¹ is shown in Figure S12c. An irreversible capacity contribution was observed during first discharge. This irreversible capacity contribution could be attributed to the rapid decomposition of electrolyte and formation of solid electrolyte interphase (SEI) at lower potential as observed from the first scan of cyclic voltammetry. The **TFPB-TAPT** COF exhibited an initial reversible discharge capacity of 398 mA h g⁻¹ at 3rd cycle with a coulombic efficiency of 98% and an as much as high specific discharge capacity of 365 mA h g⁻¹ (91.7% capacity retention) was observed after 50 cycles. Since the theoretical capacity of **TFPB-TAPT** COF is 233 mA h g⁻¹, at least 165 mA h g⁻¹ of capacity contributed from the reversible insertion of Li⁺ ion into super P carbon additive^{3,4}. Figure S12d reveals the rate performance of **TFPB-TAPT** COF at the different current rates of 30, 50, 100 and 200 mA g⁻¹, respectively. The observed capacities at different current rates were found to be extremely stable.

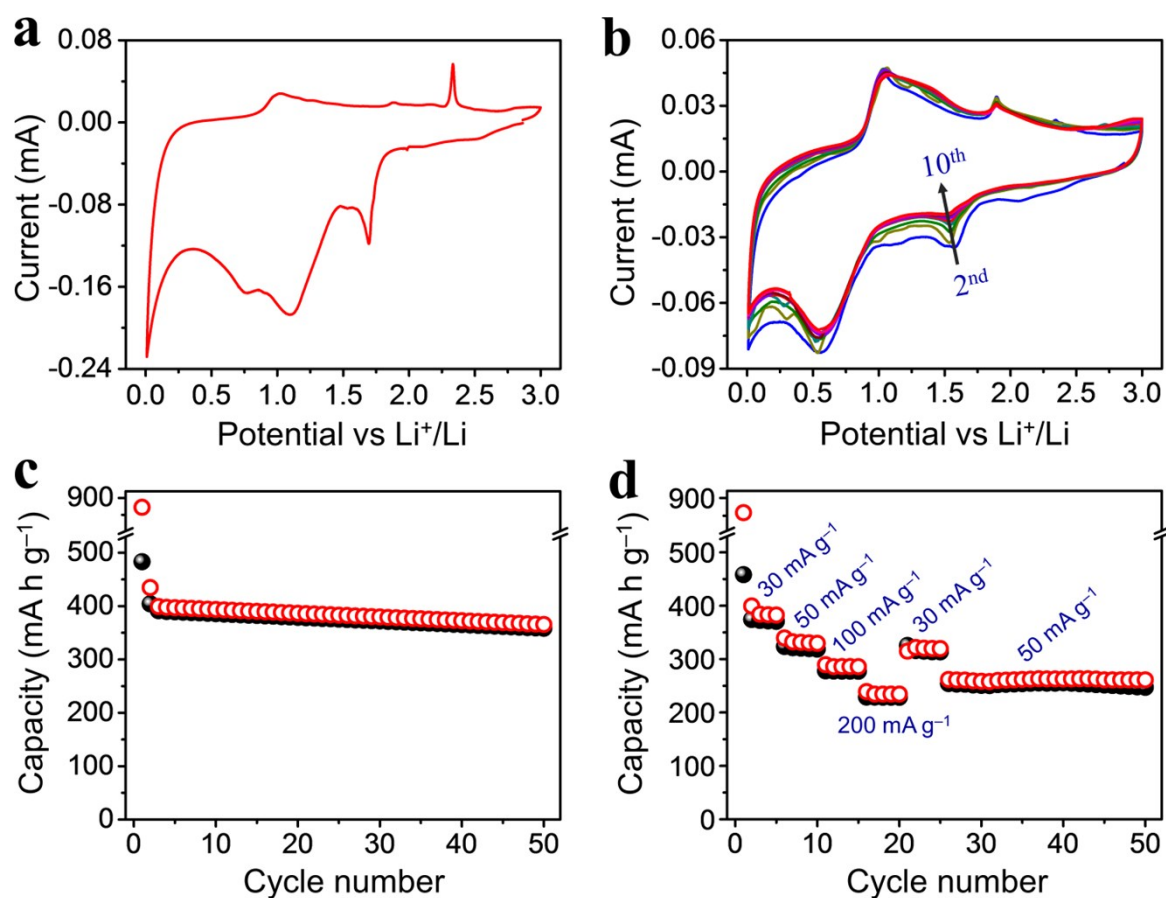


Figure S12. Electrochemical performances of TFPB-TAPT COF with respect to Li⁺/Li – (a) First cycle CV scan at the scan rate of 0.02 mV s⁻¹. (b) 2nd to 10th cycle CV scans at the scan rate of 0.02 mV s⁻¹. (c) Charge-discharge cycling performance at 30 mA g⁻¹. (d) Rate performance at the current rates of 30, 50, 100, and 200 mA g⁻¹.

References:

- [1] S. Wang, Q. Wang, P. Shao, Y. Han, X. Gao, L. Ma, S. Yuan, X. Ma, J. Zhou, X. Feng, B. Wang, *J. Am. Chem. Soc.* 2017, **139**, 4258-4261.
- [2] J. Qian, Y. Xiong, Y. Cao, X. Ai, H. Yang, *Nano Lett.* 2014, **14**, 1865-1869.
- [3] E. C. Martinez, J. C. Gonzalez, M. Armand, *Angew. Chem. Int. Ed.* 2014, **53**, 5341-5345.

[4] R. M. Gnanamuthu, C. W. Lee, *Mater. Chem. Phys.* 2011, 130, 831-834.